

Particle Acceleration in Solar Flares and Associated CME Shocks

Vahé Petrosian^{1,2}

¹*Department of Physics and KIPAC, Stanford University, Stanford, CA 94305, USA*

²*Department of Applied Physics, Stanford University, Stanford, CA 94305, USA*

ABSTRACT

Observations relating the characteristics of electrons seen near Earth (SEPs) and those producing flare radiation show that in certain (prompt) events the origin of both population appears to be the flare site, which show strong correlation between the number and spectral index of SEP and hard X-ray radiating electrons, but in others (delayed), which are associated with fast CMEs, this relation is complex and SEPs tend to be harder. Prompt event spectral relation disagrees with that expected in thick or thin target models. We show that using a more accurate treatment of the transport of the accelerated electrons to the footpoints and to the Earth can account for this discrepancy. Our results are consistent with those found by Chen & Petrosian (2013) for two flares using non-parametric inversion methods, according to which we have weak diffusion conditions, and trapping mediated by magnetic field convergence. The weaker correlations and harder spectra of delayed events can come about by re-acceleration of electrons in the CME shock environment. We describe under what conditions such a hardening can be achieved. Using this (acceleration at the flare and re-acceleration in the CME) scenario we show that we can describe the similar dichotomy that exists between the so called impulsive, highly enriched (³He and heavy ions) and softer SEP events, and stronger more gradual SEP events with near normal ionic abundances and harder spectra. These methods can be used to distinguish the acceleration mechanisms and to constrain their characteristics.

Subject headings: acceleration of particles–Sun: flares–Sun: particle emissions –turbulence–shocks

1. INTRODUCTION

Solar flares accelerate electrons and ions with varied characteristics deduced either from direct observations of the intensity, spectrum and composition of solar energetic particles (SEPs) by near Earth instruments or indirectly from the radiation they produce while interacting with background solar particles and fields. Electrons produce hard X-rays (HXR) via nonthermal bremsstrahlung (NTB) and microwaves via synchrotron mechanisms in the lower solar atmosphere and type III (and other radio) bursts in the upper corona and beyond. Accelerated protons (and other ions) interacting with background ions result in de-excitation nuclear lines in the 1 to 7 MeV range, neutrons, and pions which decay into (mainly) > 70 MeV gamma-rays. However, most of the energy of $< \sim 100$ MeV electrons and $< \sim 1$ GeV protons goes into heating and evaporation of the flare plasma which then gives rise to thermal radiation from soft X-rays (SXR) to sub-millimeter range. There are two possible acceleration sites; one in the low solar corona, where reconnection seems to be the energizing mechanism, and the other at higher corona and up to several solar radii from the Sun in the environment of the coronal mass ejection (CME), possibly by a shock and mediated by turbulence. An important question is whether radiating particles and SEPs are accelerated at only one

of these or at both sites, and if there are observations which can answer this question and shed light on the characteristics of the two acceleration mechanisms. This is the main goal of the work presented here.

In the case of SEP ions this dichotomy has manifested itself in the differences between shorter duration or more impulsive events which show large enhancement of ^3He and heavy ions and longer duration or more gradual events with photospheric abundances and harder spectra (see e.g. Mason et al. 2000 & 2002; Reames et al. 1994, 1997; Ng & Reames 1994. For a more recent review see Reames 2013). The former appear to originate from the flare site and stochastic acceleration by turbulence can account for their softer spectra and extreme enhancement of ^3He (Liu et al. 2004, 2006). The gradual events, in addition to being harder, tend to be stronger and have near normal photospheric abundances. Stochastic acceleration by turbulence has often been considered to be the mechanism of production of these SEPs (for observational evidence see e.g. Mason et al. 1986; Mazur et al. 1992; and theoretical interpretations see Miller et al. 1996; Miller 2003). However, since the gradual events are often associated with fast CMEs, and it is generally believed that the CME driven shock plays a major role in acceleration of these SEPs (see e.g. Zank 2012 Jokipii & Giacalone 1996). As described in §3, SEP electron observations also point out to presence of more impulsive type flares with close association with type III bursts and other flare emissions, and gradual flares with a less defined relation with radiative signatures and strong association with proton rich SEPs (Krucker et al. 1999; Haggetry & Roelof 2002; Maia & Pick 2004; Klein et al. 2005; Krucker et al. 2007).

High spatial resolution observations in the HXR regime by *Yohkoh*; (Masuda et al. 1994; Petrosian et al. 2002) and by the *Ramaty High Energy Solar Spectroscopic Imager (RHESSI)* (Lin et al. 2002; Krucker & Lin 2008; Liu et al. 2008), and few cases in gamma-rays by *RHESSI* (Hurford et al. 2003) and by the *Fermi Gamma-ray Observatory (Fermi)* (Ajello et al. 2013) have established that the nonthermal radiations produced by both electrons and ions originate in and below the corona. Typically HXR and gamma-ray producing particles must traverse column depths of $> 10^{20}$ and $> 10^{24} \text{ cm}^{-2}$, respectively, which are reached below the transition region and below the photosphere. It is generally believed that electrons that produce the microwaves and HXRs are accelerated in or near the reconnection region in the low corona, possibly just above the top of the flaring loops. These emissions normally are limited to the impulsive phase of a flare that lasts few seconds to several minutes. The impulsive HXR emissions are sometimes associated with high energy SEP electrons observed near the Earth (see e.g. Wang et al. 2012).

The relation of the characteristics of these electrons with those producing the HXRs depends on whether we are dealing with impulsive-prompt or gradual-delayed SEP events. The differences between these two populations can also shed light on the acceleration site and mechanism. This will be the primary focus of this paper.

The seed particles accelerated at the reconnection site in the low corona are expected to be the background plasma particles but the characteristics of seed particles to be accelerated by the shock in the gradual events are not known. In this paper we explore a scenario where the flare accelerated ions and electrons are the seeds that are re-accelerated in the CME environment of the gradual-delayed events.

In general, gamma-ray observations, in particular those by *Fermi*, point to a more complicated picture than that derived from HXR observations. Flare emitted gamma-rays were observed first by the gamma-ray spectrometer (GRS) on board the *Solar Maximum Mission (SMM)* (Chupp et al. 1982) and later by the instruments, notably EGRET, on the *Compton Gamma-ray Observatory (CGRO)*, showing both impulsive and long duration de-excitation lines and pion decay emissions (see review by Chupp & Ryan 2009). But observations by the *Fermi* gamma-ray burst monitor (GBM) and the large area telescope (LAT), with a superior sensitivity and spatial resolution, have provided new insights and raised new questions.

Some flares, like the June 12, 2011 (see Ackermann et al. 2012) show simultaneous HXR and gamma-ray impulsive emissions indicating acceleration of both electrons and ions in the low corona. But, as shown in Ackermann et al. (2014), a majority of *Fermi* flares show long duration (> 100 MeV) emission lasting sometimes over 10 hours after the impulsive phase. There does not seem to be any other associated emissions during the extended phase, but most of these flares are associated with fast CMEs and significant flux of SEPs. Irrespective of whether the extended emission is NTB by relativistic electrons or from decay of pions produced by > 320 MeV protons (and other ions), acceleration in the CME shock may be at work here as well. This possibility has gained further support from *Fermi* observations of significant impulsive and extended gamma-ray emission from several flares located behind the limb (BTL) as deduced from *STEREO* observations (Pesce-Rollins et al. 2015).

In the next section we describe the details of the combined model of acceleration in the corona and re-acceleration at the shock. We apply this to explain the relation between impulsive and gradual events as observed for electrons in §3 and He ions in §4. A brief summary and discussion is given in §5.

2. COMBINED FLARE AND CME SHOCK ACCELERATION MODEL

Our basic model for acceleration is shown in Figure 1. The left panel shows a cartoon of the model for acceleration, transport and radiation at the X-reconnection site in the corona. Acceleration can be by the second order Fermi (or stochastic) acceleration by turbulence (see e.g. Petrosian & Liu 2004), by a standing shock produced by the down flow from the X-reconnection site (see e.g. Guo & Giacalone 20120), or in the merging of islands shown to arise in PIC simulations during reconnection (Drake et al. 2006 & 2013; Le et al. 2012; Oka et al. 2013). The latter model has been invoked as a possible mechanism in the downstream of the CME shock (le Roux et al. 2015; Zank et al; 2015). The right panel shows a similar cartoon for acceleration in the environment of the CME. The (red) rectangles shows the cross section of the box within which particles are accelerated. For our purposes here the relevant parameters of the acceleration and transport of particles are the momentum (p) and pitch angle cosine (μ) diffusion rates D_{pp}/p^2 and $D_{\mu\mu}$, and direct energy gain $A(E)$ and loss \dot{E}_L rates, where E is the particle energy.¹ For an isotropic pitch angle distribution or for the gyro phase and pitch angle averaged particle energy distribution $f(t, s, E)$, where s is distance along field lines, integrated over the volume V of the acceleration site with cross section area $A(s)$, namely $N(t, E) = \int A(s) ds f(t, s, E)$, is governed by the so-called leaky-box model kinetic equation (see Petrosian 2012)

$$\frac{\partial N}{\partial t} = \frac{\partial}{\partial E} \left(D_{EE} \frac{\partial N}{\partial E} \right) - \frac{\partial}{\partial E} [(A - \dot{E}_L)N] - \frac{N}{T_{\text{esc}}} + \dot{Q}, \quad (1)$$

where \dot{Q} is a source term, $D_{EE} = v^2 D_{pp}$, and the direct acceleration coefficients for stochastic and shock accelerations are given as

$$A_{\text{SA}} = \xi \frac{D_{EE}}{E}, \quad \text{and} \quad A_{\text{sh}} = \zeta E \left(\frac{u_{\text{sh}}^2}{4\kappa_{ss}} \right) = \zeta E \left(\frac{u_{\text{sh}}}{v} \right)^2 \left(\left\langle \frac{(1 - \mu^2)^2}{D_{\mu\mu}} \right\rangle \right)^{-1}. \quad (2)$$

Here u_{sh} is the shock velocity, κ_{ss} is the coefficient of spatial diffusion (along the field lines), $\xi = (2\gamma^2 - 1)/(\gamma^2 + \gamma)$, γ is the Lorentz factor, and ζ depends on the shock compression ratio and other factors (see,

¹Here and in what follows we neglect the effects of the third diffusion coefficient $D_{\mu p}$ which are generally small (see Schlickeiser 1989; Petrosian & Liu 2004)

e.g. Steinacker et al. 1988). The energy loss rate at low energies (for both electrons and ions) is dominated by Coulomb collisions with background particles (mainly electrons).² At higher energies (not relevant for the discussion here) inelastic interactions (synchrotron, inverse Compton and bremsstrahlung) for electrons and (nuclear line excitation, neutron and pion productions) for ions become important.

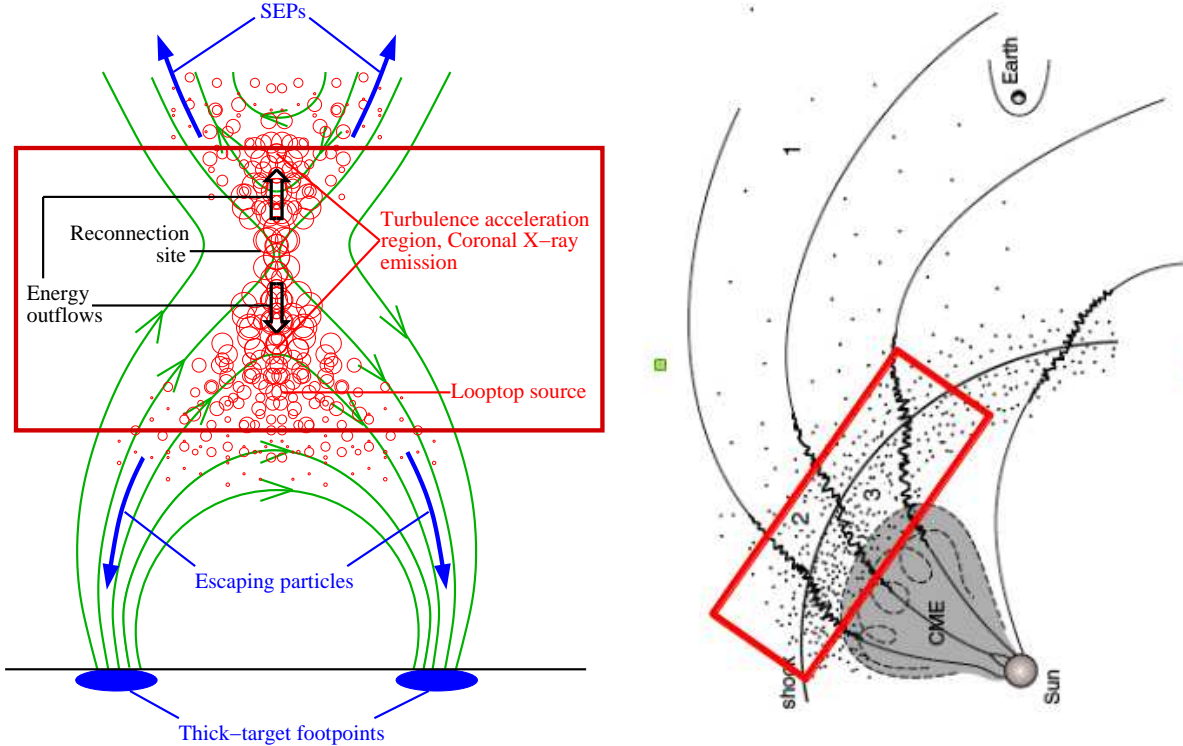


Fig. 1.— **Left:** A schematic representation of the reconnecting field (solid green) forming closed coronal loops and open field lines presumably extending into higher corona and the solar wind. The red foam represents turbulence. Acceleration probably takes place in the outflow regions above and below the X-point. Particles (temporarily) trapped here produce the radiation seen above the closed loops and particles escaping these regions up and down (blue arrows) are observed at one AU as SEPs and produce the nonthermal radiation (mainly at the two foot points; blue ovals), respectively. (From Liu et al. 2013) **Right:** A similar schematic joining the flare site field lines to the CME, the shock and beyond (from Lee, 2005). The rectangles define the boundary of the acceleration sites and represent the leaky box.

The final coefficient in Equation (1), namely the energy dependence of the escape time, has a more complicated relation to the transport coefficients and the crossing time $\tau_{\text{cross}} \equiv L/v$, where $L = V/\bar{A}$ is the average size of the acceleration site. If there is a weak or no trapping of the particles in the acceleration site; i.e. when magnetic field lines are nearly uniform and we are dealing with the *weak diffusion limit* with scattering time $\tau_{\text{sc}} \gg \tau_{\text{cross}}$ (or mean free path $\lambda_{\text{sc}} \gg L$), then the particles free stream and escape within

²Coulomb collision also cause pitch angle scattering, and therefore spatial diffusion along the field lines, with a rate that is comparable to energy loss rate at nonrelativistic energies but decreases as $1/(\gamma^2 - 1)$. They also cause energy diffusion which is negligible in the cold target case ($E \gg kT$), but can be comparable to the energy loss rate for a hot target as E approaches kT (see Petrosian & Kang 2015), where T is the background plasma temperature.

$T_{\text{esc}} \sim \tau_{\text{cross}}$. However, the relatively strong HXR emission observed near the top of many flaring loops (and not from the legs of the loops; see Masuda et al. 1994; Petrosian et al. 2002) points to the presence of some trapping of particles. This can happen in the *strong diffusion limit* with $\tau_{\text{sc}} \ll \tau_{\text{cross}}$, which is one of the requirements for establishing an isotropic momentum distribution. Scattering by turbulence is the most likely source of such trappings.³ In this case the escape time is determined primarily by the spatial (and other, see Petrosian 2012) diffusion coefficient κ_{ss} as⁴

$$(T_{\text{esc}})^{-1} = -\frac{1}{N(t, E)} \int \mathcal{A}(s) ds \frac{\partial}{\partial s} \left(\kappa_{ss} \frac{\partial f(t, s, E)}{\partial s} \right). \quad (3)$$

If we use the approximation $\partial f(t, s, E)/\partial s \sim f/L \sim N(t, E)/(VL)$ then the escape time can be written as

$$T_{\text{esc}} = \frac{\tau_{\text{cross}}^2}{\tau_{\text{sc}}} \quad \text{where} \quad \tau_{\text{sc}} \equiv 3 \frac{\kappa_{ss}}{v^2} = \frac{3}{4} \left(\left\langle \frac{(1 - \mu^2)^2}{D_{\mu\mu}} \right\rangle \right). \quad (4)$$

Combining these two limiting cases we can write $T_{\text{esc}} = \tau_{\text{cross}} (1 + \tau_{\text{cross}}/\tau_{\text{sc}})$. However, recently Chen & Petrosian (2013) (CP13), using “regularized” inversion technique of Piana et al. (2007), have determined the energy dependence of all the coefficients of the kinetic Equation (1) directly and non-parametrically from *RHESSI* observations for two flares. These results are presented as the crossing time τ_{cross} , energy loss time $\tau_L = E/\dot{E}_L$, energy diffusion time $\tau_{\text{diff}} = E^2/D_{EE}$ and the escapetime T_{esc} . From these and the above relation between escape and scattering time they obtain the variation with E of scattering time τ_{sc} and direct acceleration time $\tau_{\text{ac}} = E/A(E) \sim p^2/D_{pp}$ for both shock and stochastic acceleration. The upshot of this work is that the deduced energy dependences of the scattering and acceleration times do not agree with those calculated by Pryadko & Petrosian (1997) (PP97) based on interactions of electrons with turbulence with varied characteristics (see Fig. 5 in CP13). This suggests that strong diffusion may not be the source of the trapping.

Transport and trapping of particles in the acceleration site can also be affected by *magnetic field convergence* from the middle of the acceleration site to where they escape at its boundaries. Such a field geometry, shown for the toy model (Fig. 1 left), seem to be present in some observed loops (Liu et al. 2013). Particles will then bounce between mirror points but eventually, even in the weak diffusion limit, they will be scattered into the loss cone and escape, so that we expect $T_{\text{esc}} \propto \tau_{\text{sc}}$. Such a relation will yield a scattering time consistent with the acceleration and energy diffusion times deduced by CP13. Malyshkin & Kulsrud (2001) using some analytic treatment and numerical simulations, suggest an approximate form for the relation between the escape and scattering times which can be summarized as

$$T_{\text{esc}}/\tau_{\text{cross}} = c_1 + c_2(\tau_{\text{cross}}/\tau_{\text{sc}}) + c_3(\tau_{\text{sc}}/\tau_{\text{cross}}). \quad (5)$$

This equation combines the strong diffusion case ($\tau_{\text{sc}} \ll \tau_{\text{cross}}$) with $c_2 \sim 1$ and $c_1 = c_3 = 0$, and the weak diffusion case ($\tau_{\text{sc}} \gg \tau_{\text{cross}}$) with $c_1 \sim 1, c_2 = 0$. In the latter case $c_3 \sim 1$ for uniform field lines and increase with increasing degree of field convergence. Figure 2 shows some examples of the variation of escape time with the scattering time (both in units of crossing time), where following Malyshkin & Kulsrud (2001) we have set $c_1 = \eta, c_2 = 1$ and $c_3 = \ln \eta$ with $\eta = B_L/B_0$ the ratio of magnetic field strengths at the edge to that at the center of the acceleration site.

³Scattering by Coulomb collisions cannot be this agent because it is slower than Coulomb energy loss rate so particles lose energy as fast as or faster than they scatter (see Petrosian & Donaghy 1999). Also as shown by Chen & Petrosian (2013) Coulomb times are in general longer than all the other times associated with the transport coefficients.

⁴For other less important components of this relation see Petrosian (2012).

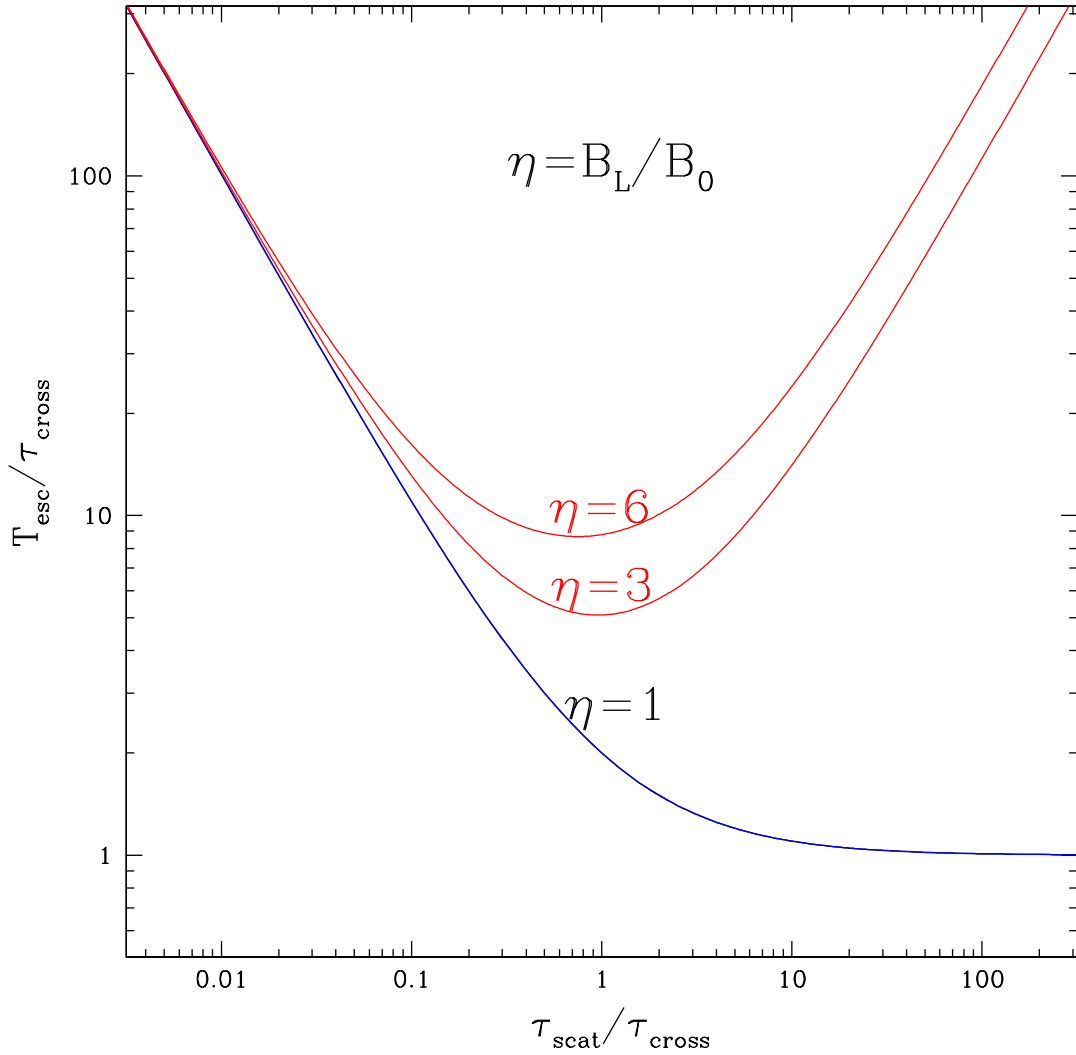


Fig. 2.— Variation of the escape time with scattering time according to Equation (5) with $c_1 = \eta$, $c_2 = 1$ and $c_3 = \ln(\eta)$ for three different degrees of field convergence parametrized by η the ratio of magnetic field from the center to the edges of the acceleration site (size L) where particles escape.

In the next section we use the above relations to relate SEP electron spectra with those deduced from HXR observations.

3. SEP AND HXR EMITTING ELECTRONS

The relation between energetic electrons observed near the Earth, with a velocity dispersion that indicates their origin from the lower corona region of the Sun, and those producing the flare radiation has been subject of several studies. Because it is by now well established that type III radio bursts are produced by energetic electrons moving out from the Sun the first investigations were focused on the relation between SEP and type III electrons. Krucker et al. (1999) using observations by instruments on board the *WIND* spacecraft found two classes of events; those with same release time from the Sun as the type IIIs (**prompt events**) and those with up to half an hour delay (**delayed events**) which tend to be harder. Haggetry & Roelof (2002) using higher energy observation by instruments on board the *Advanced Composition Explorer (ACE)* spacecraft find a good association between impulsive SEP electron events and other radiative signatures but claim that the electron release time from the Sun is delayed by few minutes relative to the observed radiations (type III, microwave and SXR). They conclude that these electrons are not accelerated at the flare site but in an outgoing coronal shock. However, the claimed delays have less than 1.5 sigma significance based on statistical errors alone and there may be systematic errors such as a longer path than the assumed 1.2 AU or small amount of scattering. Maia & Pick (2004) using observations by *ACE* and the *Nancay radioheliograph*, with imaging capability, find no delay between the electron release and type III times for events that they classify as radio-simple (only type III emission) which show weak association with CMEs. On the other hand, events classified as radio-complex show variable delays and are associated with > 600 km/s CMEs. They propose “an acceleration process in the corona, at variable heights and below the leading edge of the associated” CME. Somewhat less clear picture is presented by Klein et al. (2005) who, using *Wind* and the *Nancay radioheliograph* observations, conclude that a “combination of time-extended acceleration at heights $0.5R_{\odot}$ above the photosphere with the injection of electrons into a variety of closed and open magnetic field structures explains the broad variety of timing shown by the radio observations and the in situ measurements.”

The main focus of all the above works has been the *timing issue*. More can be learned by investigation of strength and *spectral characteristics*, like hardness or power law index. Although there are some discrepancies in the above results, they seem to have one common feature which is that the impulsive electron events that appear to originate from the flare site are weaker than events with more complex timing relation that are often associated with a CME. It would be of interest to see if flare accelerated electrons show similar trends. This cannot be ascertained by study of the type III or SXR emissions. Microwave spectra would be useful but need broader (than usually available) frequency coverage in order to separate optically thin and thick portions of the spectra. They also depend on the value and geometry of the magnetic field (see Petrosian 1982). HXR spectra, on the other hand, give a more direct information about the spectra of the accelerated electrons, and for a thick target case this relation is independent of the size of the acceleration site and background plasma density. Thus, comparing the spectra of HXRs and SEP electrons can shed a greater light on the acceleration process.

Krucker et al. (2007) (K07) have carried out such an analysis using *RHESSI* HXR spectra and *WIND* electron spectra. They divide their sample into a “prompt” group, which within the statistical uncertainties have a release time in agreement with HXR start time, and “delayed” group. They find a good correlation between the spectral index δ_{SEP} of SEP electron flux and spectral index γ of HXR photon flux above 50 keV with $\delta_{\text{SEP}} \sim \gamma_{\text{HXR}} + 0.1 \pm 0.1$ for the prompt events, but for delayed events they find no clear correlation with $\delta_{\text{SEP}} < \gamma_{\text{HXR}}$ for majority of such events, i.e, a harder SEP spectrum. They also find a somewhat weaker correlation between the two fluxes with HXR observations requiring a significantly larger (by several hundred) number of radiating electrons than that observed at one AU. In Figure 3 we show the histograms

of the frequency distribution of the SEP (left) and HXR (right) indexes for delayed (dashed-black) and prompt (solid-red) events. As evident the the above difference is primarily due to the fact that SEP spectra of delayed events are harder than prompt events and not because their HXR spectra are softer. We find average indexes $\delta_{\text{SEP}}^{\text{delayed}} \sim 2.8 \pm 0.40$ vs $\delta_{\text{SEP}}^{\text{prompt}} \sim 3.6 \pm 0.46$, and $\gamma_{\text{HXR}}^{\text{delayed}} \sim 3.7 \pm 0.57$ vs $\gamma_{\text{HXR}}^{\text{prompt}} \sim 3.5 \pm 0.55$). As discussed below, this hardening of the delayed SEP events can be attributed to the re-acceleration of the flare accelerated electrons in the CME shock.

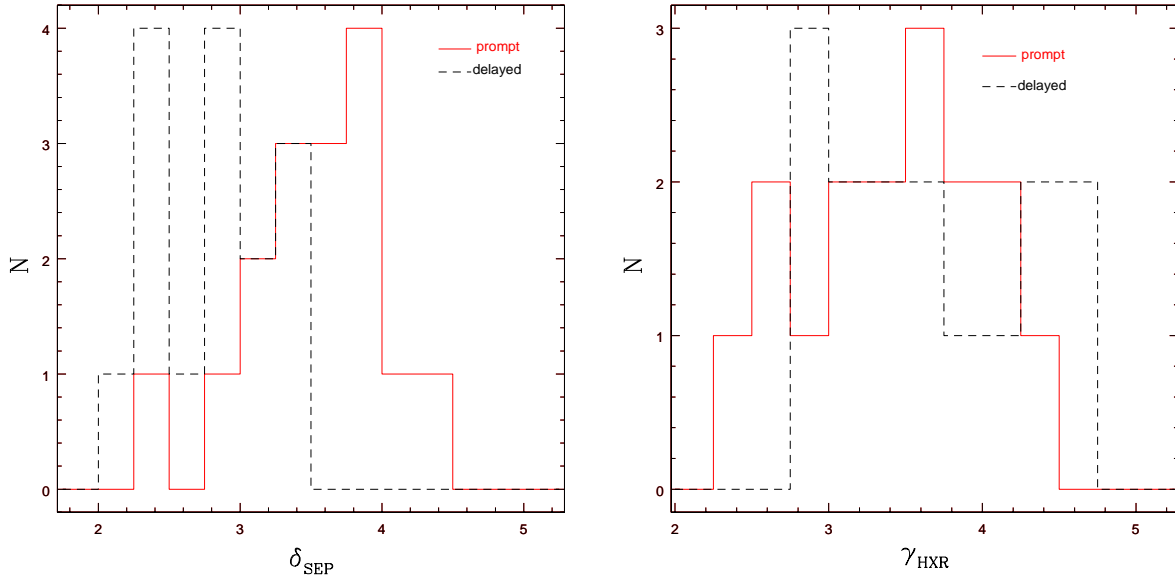


Fig. 3.— Frequency distribution of δ_{SEP} **left** and γ_{HXR} **right** for delayed (dashed-black) and prompt (solid-red) events, using the data given in K07. The average and standard deviation of the four distributions are $\delta_{\text{SEP}}^{\text{delayed}} \sim 2.8 \pm 0.40$, $\delta_{\text{SEP}}^{\text{prompt}} \sim 3.6 \pm 0.46$, $\gamma_{\text{HXR}}^{\text{delayed}} \sim 3.7 \pm 0.57$ and $\gamma_{\text{HXR}}^{\text{prompt}} \sim 3.5 \pm 0.55$.

3.1. Accelerated Electron and HXR Spectra

The relation between the NTB radiating electron and the observed HXR spectrum is relatively simple for a single source. As demonstrated some times ago this depends whether one deals with a *thin target* source, whereby electrons lose a small fraction of their energy (mostly by Coulomb collisions) while radiating, or a *thick target* source where they lose all their energy (see Lin & Hudson 1971, Brown, 1972, Petrosian 1973). The spectral index $\bar{\delta}$ of **flux** of electrons are related to the HXR index γ_{HXR} of bremsstrahlung photon flux as $\bar{\delta}_{\text{thin}} = \gamma_{\text{HXR}} - 1$ and $\bar{\delta}_{\text{thick}} = \gamma_{\text{HXR}} + 1$, respectively. As pointed out by K07 neither one of these relations agrees with observations of either the prompt (with $\delta_{\text{SEP}} \sim \gamma_{\text{HXR}}$) or delayed events where there is no clear correlations. This may indicate that the SEP and radiating electrons have different origins.

However, the assumption of single radiative source, whether thin or thick is an over simplification. First, as mentioned above, most flares show emission from a loop top source and from two (harder) footpoint sources. Second, the spectra of the electrons escaping downward, responsible for the radiation, and upwards, observed as SEPs, may be different from each other, and most likely different from the spectrum of the

accelerated electrons. Thus, the exact relation between δ_{SEP} and γ_{HXR} is more complicated and depends on the details of the acceleration and transport mechanisms. Let us consider the model for acceleration in the corona shown in the right panel of Figure 1. The (red) rectangle represents the leaky box within which the acceleration mechanism produces a spectrum $N(E)$ of electrons (integrated over the acceleration region). These electrons are responsible for the emission from the loop top source (with a background density of n_{LT}) and yield a HXR spectrum (photons per s per unit ϵ) given by

$$J_{\text{LT}}(\epsilon) = \int_{\epsilon}^{\infty} n_{\text{LT}} v N(E) \sigma(\epsilon, E) dE = \tau_{\text{br}}^{-1} \epsilon^{-1} \int_{\epsilon}^{\infty} \beta^{-1} N(E) f(\epsilon/E) dE, \quad (6)$$

where $\beta = v/c$, $\tau_{\text{br}} \equiv (16/3)r_0^2 \alpha n c$ and $f(\epsilon/E)$ is a slowly varying function.⁵ Here E and ϵ are in units of electron rest mass energy $m_e c^2$, $\alpha = 1/137$ and $r_0 = e^2/m_e c^2$. This is a *thin target* spectrum which in the nonrelativistic regime ($\beta = \sqrt{2E}$) and for a power law electron spectrum $N(E) = N_0 E^{-\delta}$ yields

$$J_{\text{LT}}(\epsilon) = \frac{N_0}{\sqrt{2}\tau_{\text{br}}} \epsilon^{-\delta-1/2} I_{\delta-3/2}(0), \quad \text{with } I_n(x) = \int_x^1 t^n f(t) dt, \quad (7)$$

so that the HXR index $\gamma_{\text{HXR}} = \delta + 1/2$. Note that in our notation δ is the index of the spectrum accelerated particles. The index for the **flux** $F = \bar{v}N$ of electrons in the nonrelativistic regime of interest here will be $\bar{\delta} = \delta - 1/2$ and the HXR index $\gamma_{\text{HXR}} = \bar{\delta} + 1$, the relation mentioned above and used in K07 and elsewhere.⁶

Most of the higher energy HXRs, however, are produced by particles escaping downward along the legs of the loop to the footpoints (see Fig. 1, left), with a total flux of $N(E)/T_{\text{esc}}^d(E)$, where they produce *thick target* NTB again given by Equation (7) but with $n_{\text{LT}}N(E)$ replaced by n_{FP} times the effective thick target spectrum (see CP13 and references cited there)

$$N_{\text{eff}}(E) = \frac{1}{\dot{E}_L} \int_E^{\infty} \frac{N(E')}{T_{\text{esc}}^d(E')} dE', \quad (8)$$

where the energy loss rate at the foot points, dominated by Coulomb collision in nonrelativistic energies, is $\dot{E}_L = 1/(\beta\tau_{\text{Coul}})$; with $\tau_{\text{Coul}} = 1/(4\pi r_0^2 n c \ln \Lambda)$ and Coulomb logarithm $\ln \Lambda \sim 20$. The total bremsstrahlung flux will be equal to the sum of the loop top and footpoint emissions. In the Appendix A we describe an inversion method where one can obtain the accelerated and effective spectra from the total spectrum for a given energy dependence of the escape time. However, for our purpose here dealing with spectra and fluxes above 50 keV the loop top emission can be ignored so we will consider the thick target footpoint spectra. For the limited range of available observation K07 fit the HXR spectra with power laws and give the indexes. As evident from Equation (7) (and Eq. (9) below), this requires a power-law accelerated electron spectrum. If we assume a power law energy dependence of downward escape time, $T_{\text{esc}}^d(E) = T_{\text{esc},0}^d (E/E_0)^{\alpha_d}$, (which seems to be a good approximation; see CP13), then it is straight forward to show that

$$J_{\text{FP}}(\epsilon) = \frac{N_0}{\delta + \alpha_d - 1} \frac{\tau_{\text{Coul}}}{T_{\text{esc},0}^d \tau_{\text{br}}} \epsilon^{-\delta-\alpha_d+1} I_{\delta+\alpha_d-3}(0), \quad (9)$$

so that the HXR spectral index is

$$\gamma_{\text{HXR}} = \delta + \alpha_d - 1. \quad (10)$$

Note that for energy independent escape time ($\alpha_d = 0$) this gives the standard thick target relation. This relation is valid both for prompt and delayed events. In the next two sections we relate these HXR spectral indexes to the SEP electron index.

⁵For nonrelativistic energies $f(x) = \ln \frac{1+\sqrt{1+x}}{1-\sqrt{1+x}}$ and for extreme relativistic regime $f(x) = (1-x+3x^2/4)[\ln(1.2\epsilon) + \ln \frac{1-x}{x^2}]$ (see Koch & Motz 1959).

⁶For the relativistic regime $\bar{\delta} = \delta$ and one gets $J(\epsilon) \propto \epsilon^{-\delta}(a \ln \epsilon + b)$; a and b order unity.

3.2. Prompt Events

Some of the accelerated electrons, those on open field line, escape upward and out of solar atmosphere with an escape time $T_{\text{esc}}^u(E)$, and are observed as SEP electrons. If they are not scattered or have not suffered any energy loss or gain, which is believed to be the case for the prompt events, then the observed SEP flux spectrum will be proportional to $N(E)/T_{\text{esc}}^u(E)$. Assuming a power law escape time (which again is a good approximation for small range of energies 50 to < 500 keV), $T_{\text{esc}}^u(E) \propto E^{\alpha_u}$, the SEP electrons will have an spectral index $\delta_{\text{SEP}} = \delta - \alpha_u$. Combining this with Equation (10) we get

$$\delta_{\text{SEP}} = \gamma_{\text{HXR}} + 1 + \alpha_u - \alpha_d. \quad (11)$$

Thus, it is clear that *the energy dependences of the escape times down to the photosphere and up into the solar wind play crucial roles in the relation between the SEP electron index and the HXR index*. Consequently, the observed indexes can be used to determine the escape time indexes α_u and α_d , and constrain the models. For example, the usual assumption used in the standard thick target model that the escape times are independent of energy (i.e. $\alpha_u = \alpha_d = 0$), lead to $\delta_{\text{SEP}} = \gamma_{\text{HXR}} + 1$, which can be ruled by the observed linear regression relation $\delta_{\text{SEP}} = \gamma_{\text{HXR}} + 0.1 \pm 0.1$ given in K07. ± 0.1 is the error on the slope and not the intercept. As evident from Figure 3 the dispersions (given in the caption) of measured spectra are larger. In what follows we use this larger error bar of ± 0.3 , which is also comparable to errors of individual index measurements. Thus, we estimate that thick and thin target models are ruled at the 3σ level.

In the **strong diffusion case** particle escape up and down is determined by the scattering and crossing time in the acceleration site which would give the same energy dependence for both escape times, $\alpha_d = \alpha_u$. This also leads to a thick-target type relation and can be ruled at about the same level.

In the **weak diffusion limit**, on the other hand, for the electrons escaping upward along *diverging* field lines we are in the $\eta = 1$, $\tau_{\text{cross}} < \tau_{\text{sc}}$ branch of Figure 2 so that $T_{\text{esc}} \sim \tau_{\text{cross}} = L/(c\beta) \propto E^{-0.5}$ at nonrelativistic energies and approaches a constant L/c in the extreme relativistic regime. More exactly $\alpha_u = -d \ln \beta / d \ln E = 1/[(E + 1)(E + 2)]$. In the energy range of interest, 50 to 200 keV this changes from -0.43 to -0.3 . In what follows we will use $\alpha_u = -0.4$. From Equation (11) we then get the average value $\bar{\alpha}_d = 0.6 \pm 0.30$. This positive index is in agreement with the energy dependence obtained by CP13 for two flares. As derived in CP13 the acceleration time also increases with increasing energy. Because, in general we expect similar energy dependence for the scattering and acceleration times (see the discussion in §2 and PP97), the above result implies that we are again in the weak diffusion limit but on the branches with $\eta > 1$. To determine the value of η we need the absolute values of the escape and scattering time. The latter depends on the intensity and spectrum of the turbulence (see the discussion below) which is unknown or at least cannot be derived from the data under consideration here. A corollary of this result is that from the analysis of this kind of data we can constrain the energy dependences of the scattering and acceleration times.

Figure 4 shows the frequency distribution of α_d we obtain from K07 observations. As also shown in this figure, the two flares for which CP13 derive the values of this index are in excellent agreement with the K07 observations. *We conclude, therefore, that the observations presented in K07 for the spectra of prompt events are consistent with the idea that the trapping of the electrons in the loop top region is caused by converging field lines from loop top to footpoint regions of the reconnecting flare loop and that we are in the weak diffusion limit.*

Next we consider the **relative numbers of observed SEP electrons and the number of radiating electrons** deduced from HXR fluxes. We first define the total spectrum of accelerated electron $N_{\text{tot}}(E) =$

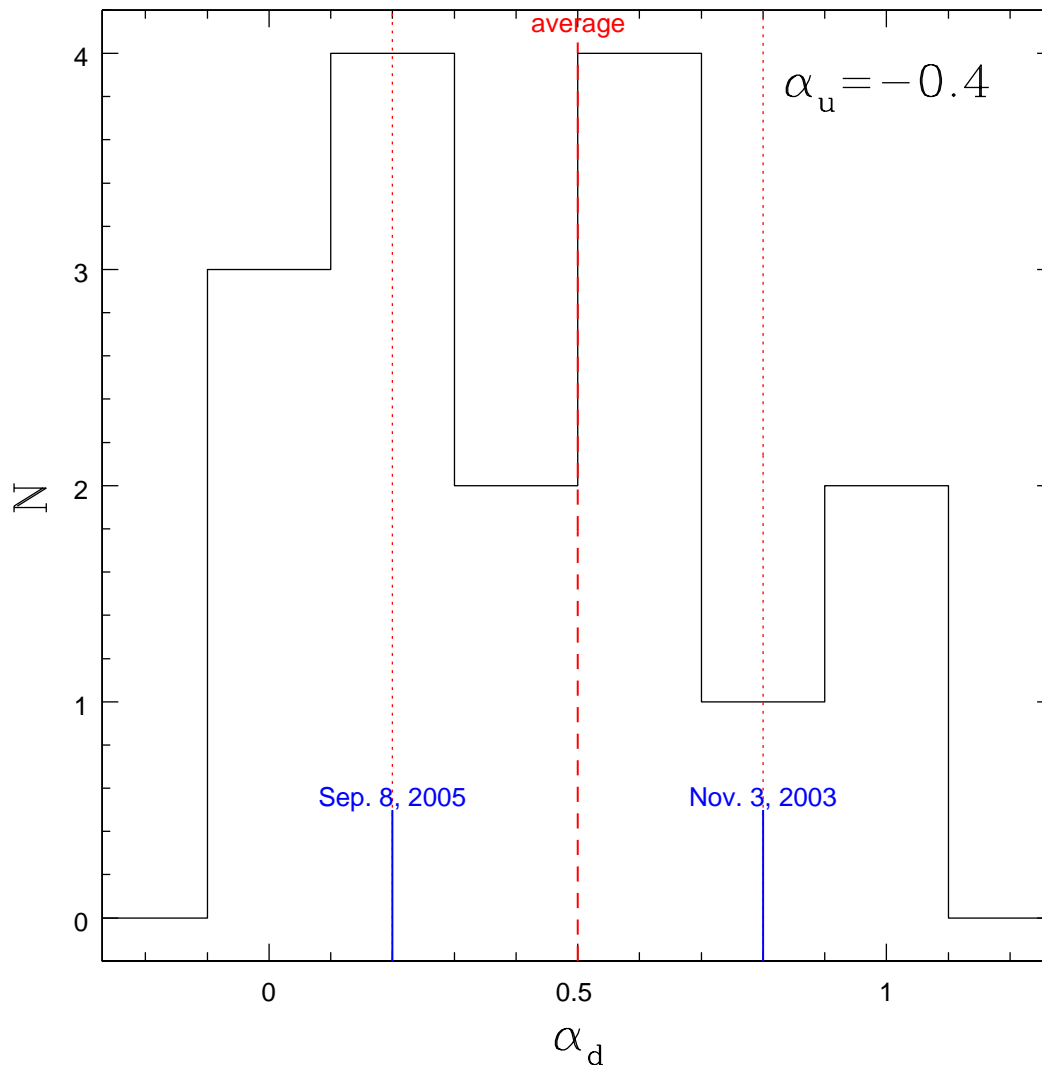


Fig. 4.— Frequency distribution of α_d , the power law index of energy dependence of the escape time downwards, based on Equation (11) and the observed values of indexes of prompt events, in the weak diffusion limit with $\alpha_u = -0.4$ (i.e. free streaming of accelerated electrons upward from the acceleration site along diverging open field lines). The dashed and dotted (red) vertical lines give the average and one sigma range of the observations. The short (blue) vertical lines show the value of a_d obtained by CP13 for two flares using an inversion method.

$\int N(E, t) dt = N(E) \Delta T$, where $N(E)$ is the average (or steady state) spectrum of electrons and ΔT is the flare duration. We express the time integrated number of SEP and HXR-producing electrons in terms of these two quantities. The expected flux of SEP electrons at Earth (distance d), after correcting for the velocity dispersion, $F_{\text{SEP}} = (N(E)/T_{\text{esc}}^u)/(\Omega d^2)$, where Ω is the steradians within which the up-escaping

electrons are directed. If one assumes that the spatial distribution of SEPs is isotropic,⁷ then the deduced number of SEP electrons above some energy E_0 (here 50 keV) will be given by

$$N_{\text{SEP}} = \left(\frac{4\pi}{\Omega}\right) \left(\frac{c\Delta T}{L_u}\right) \int_{E_0}^{\infty} \beta(E)N(E)dE = \left(\frac{4\pi}{\Omega}\right) \left(\frac{c\Delta T}{L_u}\right) N(E_0) \frac{E_0^{1-\alpha_u}}{\gamma_{\text{HXR}} - \alpha_d} \quad (12)$$

where we have defined $N(E_0) = N(E)(E/E_0)^\delta$ and $L_u = V/\mathcal{A}_u$ (with \mathcal{A}_u the cross section area of the bundle of field lines over which the particles escape to the Earth), and used the weak diffusion escape time ($\alpha_u = -d \ln \beta / \delta \ln E$) and Equation (11).

The total (volume and time integrated) number of HXR electrons are obtained from the total number of observed HXRs with energies $\epsilon \geq E_0$, which following Equation (7) can be written as

$$J(\epsilon > E_0) = \Delta T n \mathcal{A}_d \int_{E_0}^{\infty} d\epsilon \int_{\epsilon}^{\infty} F_{\text{eff}}(E) \sigma(\epsilon, E) dE = \Delta T n \mathcal{A}_d \int_{E_0}^{\infty} F_{\text{eff}}(E) dE \int_{E_0}^E \sigma(\epsilon, E) d\epsilon, \quad (13)$$

where n is the background density, \mathcal{A}_d is the area and $F_{\text{eff}}(E) = vN_{\text{eff}}(E)/V$ is the effective mean (or the steady state) flux of electrons. Inversion of this equation can give the total number of HXR emitting electrons $N_{\text{HXR}} = (\Delta T c / L_d) \int_{E_0}^{\infty} \beta N_{\text{eff}}(E) dE$, with $L_d = V/\mathcal{A}_d$. As mentioned above the thick target emission is independent of the background density so that in the above relations one can use a fiducial value for the density because the energy loss rate is $\dot{E}_L = 4\pi r_0^2 \ln \Lambda c n / \beta$ in the denominator of Equation (8) is proportional to n (for further clarification see CP13). Now substitution of the integral in (8) in the above expression (and after exchanging the order of the integrations over E' and E) we obtain

$$N_{\text{HXR}} = \frac{\Delta T c}{L_d} \frac{\tau_{\text{Coul}}(E_0)}{T_{\text{esc}}^d(E_0)} \frac{E_0^{\alpha_d-1}}{\beta(E_0)} \int_{E_0}^{\infty} \frac{N(E')}{E'^{\alpha_d}} dE' \int_{E_0}^{E'} \beta^2 dE, \quad (14)$$

where we used the power law approximation for the escape time [$T_{\text{esc}}(E) = T_{\text{esc}}(E_0)(E/E_0)^{\alpha_d}$]. In the non relativistic limit, $\beta^2 \sim 2E$, Equations (12) and (14) give the ratio

$$R_N = \frac{N_{\text{HXR}}}{N_{\text{SEP}}} = \left(\frac{\Omega}{4\pi}\right) \left(\frac{L_u}{L_d}\right) \left(\frac{\tau_{\text{Coul}}(E_0)}{T_{\text{esc}}^d(E_0)}\right) \left(\frac{\gamma_{\text{HXR}} - \alpha_d}{(\gamma_{\text{HXR}} + \alpha_u)(\gamma_{\text{HXR}} + \alpha_u - 2)}\right). \quad (15)$$

The primary term here is the ratio of the the Coulomb to escape time which for the two flares measured by CP13 is about 10 but increases with decreasing value of the loop top density.. The first term in the ratio depends on the spatial anisotropy of the SEP electrons which is is not well-known and could be close to unity. The last term for $\alpha_u = -0.4$ and for the observed range of α_d shown in Figure 4 varies from about 0.5 to 10. The final term $L_u/L_d = \mathcal{A}_d/\mathcal{A}_u$ depends at what point the acceleration stops below and above the X-point reconnection. This ratio is most likely smaller than 1. The factor of 10 derived here is smaller than the observed ratios of about several hundred, indicating perhaps that densities are about 10 times lower than $n_{\text{LT}} \sim (2-5) \times 10^{10} \text{cm}^{-3}$ used in CP13, or that a smaller fraction of upward escaping electrons are on field lines with good connection to the Earth.

3.3. Delayed Events and Re-acceleration

As shown in Figure 3, the SEP spectra of delayed events on average are harder than those of the prompt events and also harder than that of the associated HXR producing electrons. Moreover, the correlation

⁷Note that the velocity distribution of on diverging field lines will be peaked around the direction of the field lines. But since we are dealing with pitch angle integrated quantities this does not affect the results presented here.

between δ_{SEP} and γ_{HXR} is not as strong as that in the prompt events. The temporal relation of SEPs and HXRs and the weak correlation between their indexes (see bottom panel of Fig. 3 in K07) indicate some connection between the SEPs and HXRs in the delayed events as well. As shown in Figure 5 for several events $\gamma_{\text{HXR}} \sim \delta_{\text{SEP}} + 1.5$ indicating that $\alpha_d = \alpha_u + 2.5 > 2$. In the weak diffusion limit this will require a turbulence spectrum that is much flatter than kolmogorov and in the strong diffusion limit a very steep spectrum. Thus, this behavior may be an indication of presence of a different acceleration process. Since delayed-gradual events are more likely to be associated with Type II radio bursts and/or CMEs, then it is natural to assume that the SEPs in these events are accelerated in the CME shock.

The nature and origin of the seed particles in shock acceleration in general, and for production of SEPs in CME shocks in particular, is not well known. It is sometimes assumed to be a preexisting nonthermal component in the solar wind with a *kappa* type distribution, or particles trapped behind an earlier (slower) CME (see e.g Parker & Zank 2012; Tylka & Lee 2006 and references therein). In these and most other scenarios of SEP acceleration in a CME shock the seed particles come from the upstream region of the shock. Here we consider an alternative model where seed particles come from the downstream region. Because of the strong temporal relation, the weak spectral correlation and consistently harder spectra of the delayed events we are lead to consider a scenario where the SEP spectra result from re-acceleration of flare site electrons. This re-acceleration is the cause of the harder SEP than HXR producing electron spectra in these events.⁸ An important assumption here is that the CME launch and acceleration of the electrons at the reconnection are almost simultaneous, and/or the upward escaping accelerated electrons are trapped by turbulence (or other means) in the downstream region of the shock. As described in §3.2 we need only a small fraction of these electrons to be trapped and re-accelerated, which renders this assumption reasonable.

In order to treat the re-acceleration we must now consider the solution of the kinetic Equation (1) in the leaky box depicted on the right panel of Figure 1, where now the source term is the spectrum of particles escaping upward from the Sun; $\dot{Q}' = N(E)/T_{\text{esc}}^u(E)$, which we assume to be a power law with index $\delta_{\text{SEP}} \sim \gamma_{\text{HXR}} + 0.1$ as in the prompt events.⁹ The background plasma conditions in the CME shock is quite different than that in the flare loop. Both magnetic field and density are lower and decrease with increasing distance from the Sun. Gopalswamy & Yashiro (2011) using the observed sizes and radii of the CME and the shock, and theoretical model of Russell & Mulligan (2002), derive an Alfvén Mach number $\mathcal{M}_A \sim 2$ and Alfvén velocity $v_A \sim 500$ km/s. From this they estimate the plasma density and magnetic field values and variations with distance. At a distance of 2 to 3 solar radii (from the center of the Sun) they give $B \sim 0.1$ G and $n \sim 10^5$ cm⁻³. This implies a low energy loss rate or energy loss times $\tau_L > 10$ days so that the loss term in Equation (1) can be ignored. Let us first assume that the acceleration by the CME driven shock is the dominant mechanism here in which case we can ignore the energy diffusion term and obtain the kinetic equation for the steady state case as

$$d(A'N')/dE + N'/T'_{\text{esc}} = \dot{Q}'. \quad (16)$$

If we define $d\eta = dE/(T'_{\text{esc}}A')$ we obtain the formal solution for the flux of escaping electrons

$$F'(E) = \frac{N'(E)}{T'_{\text{esc}}(E)} = \frac{\mathcal{R}(E')}{E} \int_{E_0}^E e^{\eta(E') - \eta(E)} \dot{Q}'(E') dE', \quad (17)$$

⁸Note that a shock, or for that matter any other mechanism, does not always result in a harder spectrum. A seed population with a hard spectrum will be modified slightly by a mechanism with weak acceleration rate; see e.g Forman, Webb & Oxford (1981). As we will show below in our case dealing with relatively soft (flare accelerated) seed particles, a reasonable rate of acceleration can lead to a harder spectrum.

⁹In what follows we will use primed quantities for the re-acceleration process.

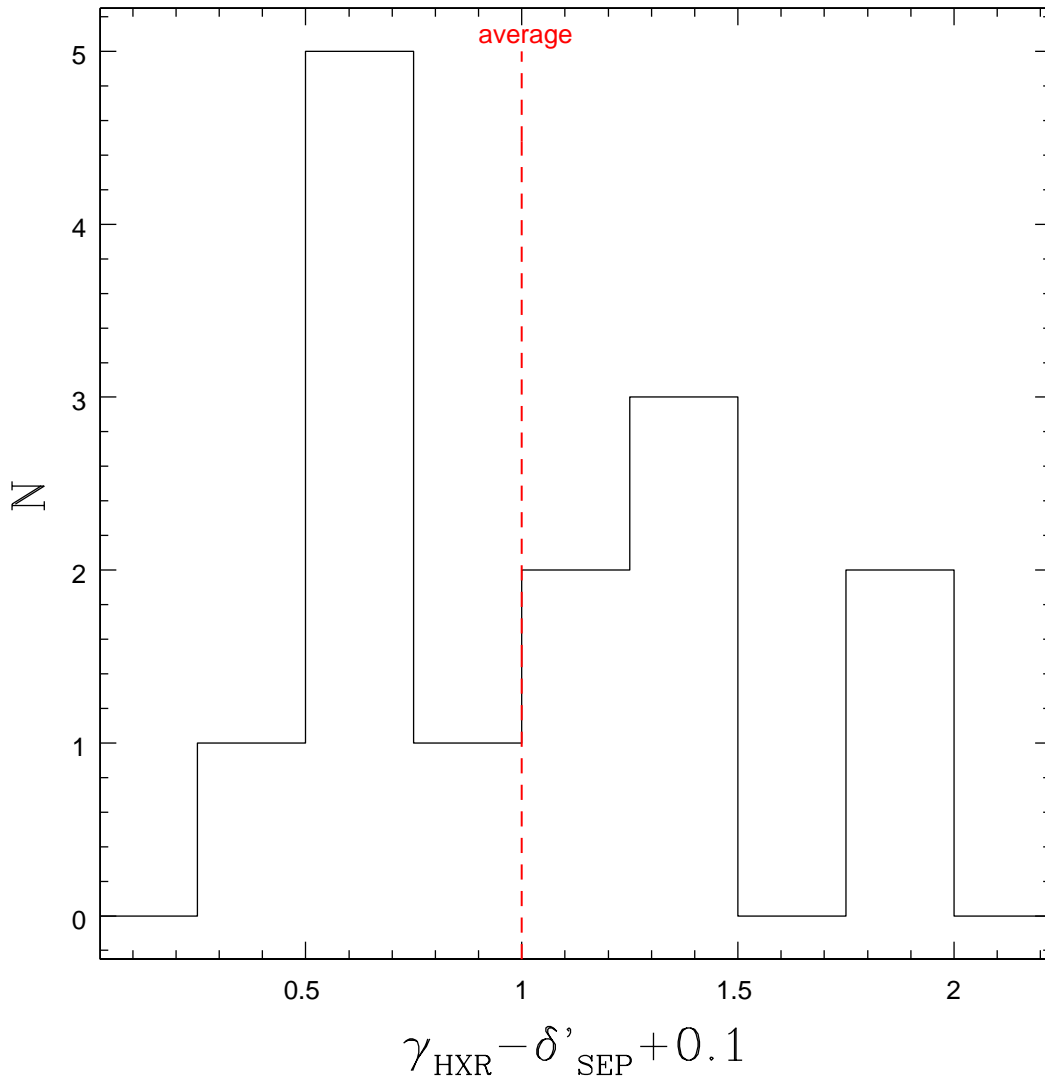


Fig. 5.— Frequency distribution of degree of hardening observed in delayed SEPs compared to prompt events. We assume that the electrons escaping the acceleration site have an spectral index $\delta_{\text{ESP}} = \gamma_{\text{HXR}} + 0.1$, thus this represent the difference in the index of the electrons escaping the flare site and the index of those escaping the CME environment after re-acceleration there. This change of index is related to the index $r \equiv d \log \mathcal{R}(E)/d \log E$.

where E_0 is a fiducial value of energy below which the approximations used breakdown and we have defined

$$\mathcal{R}(E) = \frac{E}{A T'_{\text{esc}}} = \frac{\tau'_{\text{ac}}(E)}{T'_{\text{esc}}(E)} \quad \text{and} \quad \eta(E') - \eta(E) = \int_E^{E'} \mathcal{R}(x) d \ln x. \quad (18)$$

As shown in Appendix B a slightly different version of this solution provides a good approximation for stochastic acceleration scenario too.

The solution of this integral is governed by the energy dependence of the ratio of acceleration time to escape times $\mathcal{R}(E)$. If for all relevant energies $\mathcal{R}(E) \gg 1$ the electron escape at a faster rate than they are accelerated. Thus, there will be little re-acceleration and the escaping electrons from the CME environment will have the same spectrum as the injected electrons escaping the flare site; $F'(E) = \dot{Q}'(E)$, and have the same spectral index; $\delta'_{\text{ESP}} = \delta_{\text{ESP}}$. This result also can be derived from Equation (17) by noting that in this case $\eta(E) \sim \mathcal{R} \gg 1$ so that most of the contribution to the integral comes from the upper limit of the integrand; $\int_{E_0}^E \dots \sim \dot{Q}' dE/d\eta = A'(E)T'_{\text{esc}}(E)\dot{Q}'(E)$. In the opposite extreme case, $\eta(E) \sim \mathcal{R}(E) \ll 1$, particles undergo considerable acceleration before they escape. In this case the exponential terms in Equation (17) are about one, and for $\delta_{\text{SEP}} > 1$, which is the case here, most of the contribution to the integral comes from the (constant) lower bound of the integral, so that the integral is essentially independent of the energy spectrum of the injected flux and the re-accelerated flux $F'(E) \propto E^{r-1}$, where $r \equiv d \log \mathcal{R}/d \log E$. As shown in Appendix C this change of spectrum with \mathcal{R} can be seen clearly for the special case of $r = 0$, i.e. when τ_{ac} and T_{esc} have similar energy dependences, where one can get an analytic solution. These behaviors is also evident in Figure 6, where we present re-accelerated fluxes ($F'(E)/[\dot{Q}'(E_0)\mathcal{R}_0]$) from numerical evaluations of Equation (17) for two values of the spectral index of injected electron (from the flare site) and four values of the ratio $\mathcal{R}(E_0)$, at a fiducial energy $E_0 \sim 50$ keV, and two values of its exponent r .¹⁰

As evident for large \mathcal{R} and at higher energies we get spectra as steep as the injected spectra but at lower energies and lower values of \mathcal{R} we get harder spectra with index $\delta'_{\text{SEP}} \sim r - 1$, independent of injected spectrum. Therefore, in order to produce the harder spectra (change of index by 1 or 2) seen in the delayed events, we require a value of \mathcal{R} slightly less than one and an index $r \sim 1$. Higher values of this index can result in an index changes ranging from 3 to 4 in the energy range $E_0/2 < E < 5E_0$.

A more important result is that this kind of analysis can shed light on the characteristics of the re-acceleration mechanism. Below we give a brief description of the expected values of these characteristics.

3.4. Requirements of Re-acceleration

For re-acceleration to be significant we need a acceleration time somewhat shorter than the escape time, but not very much shorter because the spectral hardening will be too severe. In the CME environment, with relatively low magnetization and Alfvén velocity, the scattering time is expected to be much shorter than the acceleration time so that $T_{\text{esc}} \gg \tau_{\text{sc}}$. In the turbulent upstream and downstream of the shock this implies we are dealing with the strong diffusion case which is required for repeated passage of the electrons across the CME shock if acceleration is indeed by the shock. Short acceleration time is also required if the acceleration is directly (and stochastically) by the turbulence. From Equations (2) and (4) we obtain the stochastic and shock acceleration times $\tau_{\text{ac}}^{\text{SA}} = E/A'(E) = \zeta'\tau_{\text{ac}}$ (see Appendix B for definition of ζ') and $\tau_{\text{ac}}^{\text{sh}} = (3/4)\zeta^{-1}(v/u_{\text{sh}})^2\tau_{\text{sc}}$ from which we derive

$$\mathcal{R}_{\text{sh}}(E) = \frac{3}{4\zeta} \left(\frac{v}{u_{\text{sh}}} \right)^2 \left(\frac{\tau_{\text{sc}}}{\tau_{\text{cross}}} \right)^2 \quad \text{and} \quad \mathcal{R}_{\text{SA}}(E) = \frac{\zeta'\tau_{\text{ac}}\tau_{\text{sc}}}{\tau_{\text{cross}}^2}. \quad (19)$$

Thus, the degree of hardening due to re-acceleration is determined by the acceleration and scattering times which depend on the momentum (or energy) and pitch angle diffusion coefficients for stochastic and shock acceleration, respectively. These in turn are determined by the physical condition of the plasma (primarily

¹⁰In order to avoid divergence at low energies we use the injected spectrum $\dot{Q} = [1 + (E/E_c)^\delta]^{-1}$.

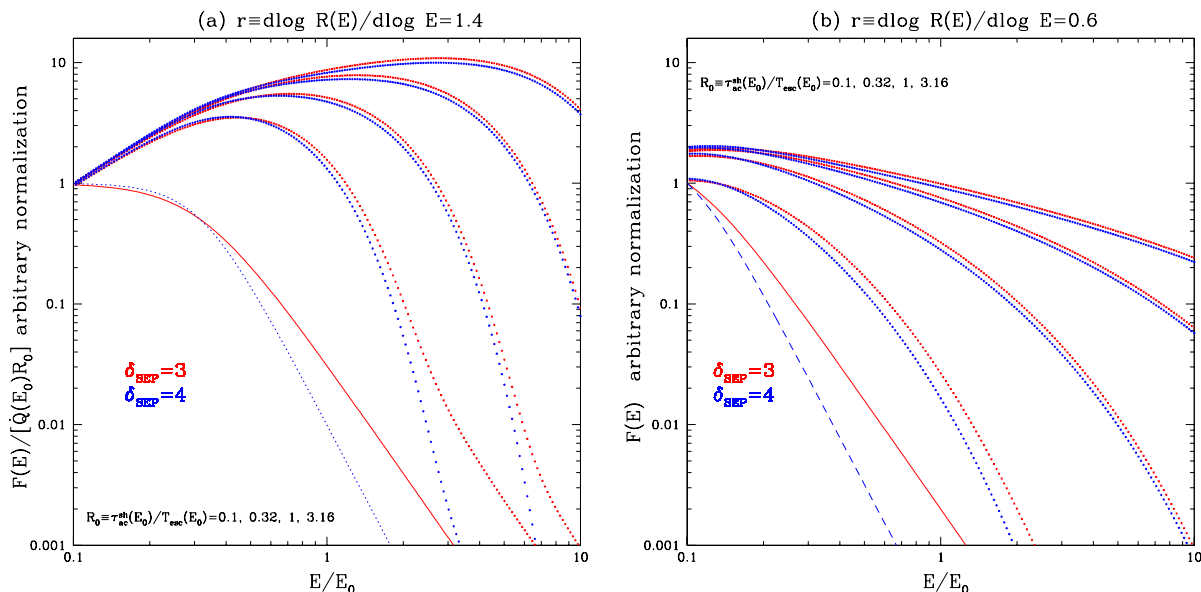


Fig. 6.— Flux of re-accelerated spectra of electrons injected by the coronal flare into the CME environment with two spectral indexes $\delta_{\text{SEP}} = 3$ (red-crosses) and $\delta_{\text{SEP}} = 4$ (blue-dots), and for two values of the index $r \equiv d \log \mathcal{R}(E)/d \log E$. Note that spectra change rapidly from no re-acceleration to highly hardened spectra for decreasing values of the ratio R from bottom to top. The two curves (solid-blue, red-dotted) show the assumed injected spectra $\dot{Q}(E) = [1 + (E/E_c)^\delta]^{-1}$, with $E_c \sim E_0/3$, chosen to avoid divergence at low energies, but to have the simple power law form in the relevant energy range $E > E_0/2$.

the Alfvén velocity $v_A = c\beta_A$), and spectral characteristics of the turbulence (primarily the spectral index q and the range of k_{\min}, k_{\max} of the k vector) in the re-acceleration site. For extreme relativistic electrons, interacting mainly with Alfvénic turbulence, these relations are simple; $\tau_{\text{ac}}^{\text{SA}} \sim \tau_{\text{sc}}/\beta_A^2 \propto \tau_p E^{2-q}$, where the characteristic rate $\tau_p^{-1} \sim \Omega_c f_{\text{turb}} (ck_{\min}/\Omega_c)^{q-1}$, with Ω_c the gyrofrequency and $f_{\text{turb}} \sim (\delta B/B)^2$ the fraction of the magnetic energy in turbulence. But at the sub- and semi-relativistic energies of interest here electrons interact with other modes of the turbulence and the relation between the two time scales and their energy dependences vary significantly with the values of q and β_A . Examples of these were presented first in Figs. 12 and 13 of PP97 (for a combined version see Fig. 5 of CP13). Note that PP97, instead of the Alfvén velocity, use the ratio of plasma to gyro frequencies $\alpha = \omega_p/\Omega_c = 1/(43\beta_A)$. Moreover, the rates calculated in PP97 are for parallel propagating waves including all cold plasma modes. Subsequent papers Pryadko & Petrosian 1998, 1999 deal with perpendicular propagating waves and hot plasma effects and obtain similar results. In what follows we will use the results for parallel propagating waves. As mentioned above in typical CME environment at a distances of $\sim 2R_\odot$ the Alfvén velocity is about 500 km/s (corresponding to $\alpha \sim 14$), and although the plasma density and magnetic field decrease rapidly with distance from the Sun, the Alfvén velocity decreases only gradually. Fitting the curves in PP97 for $\alpha = 10$ and $q = 5/3$, in the energy range 50-200 keV, we obtain $\tau_{\text{ac}}/\tau_p \sim 20E_{50}^{-0.7}$ and $\tau_{\text{sc}}/\tau_p \sim 1.0E_{50}^{-0.0}$, where $E_{50} \equiv (E/50 \text{ keV})$. From these we get the timescales

$$\frac{\tau_{\text{ac}}^{\text{sh}}(E)}{\tau_p} = \frac{0.13}{\zeta\beta_{\text{sh}}^2} E_{50}^{0.8}, \quad \frac{\tau_{\text{ac}}^{\text{SA}}(E)}{\tau_p} = 20\zeta' E_{50}^{0.7} \quad \text{and} \quad \frac{T'_{\text{esc}}(E)}{\tau_p} = 5.9 \left(\frac{L}{c\tau_p} \right)^2 E_{50}^{-0.8}, \quad (20)$$

where we have used the approximation $\beta = 0.4E_{50}^{0.4}$. These give similar \mathcal{R} 's and hardening indexes of $r_{\text{sh}} \sim 1.6$ and $r_{\text{SA}} \sim 1.5$, which as shown in Figure 6a, results in significant hardening but somewhat curved spectra. Carrying out this exercise for $q = 3$ we get index values of 0.7 and 0.4, which will give less curved spectra similar to those in Figure 6b.

We therefore conclude that the properties of the observed sample of delayed events as a whole is consistent with primary acceleration in the corona and re-acceleration in the CME environment.

To compare **stochastic vs shock acceleration** further we calculate the ratio of their rates or time scales

$$R_{\text{ac}} = \frac{\tau_{\text{ac}}^{\text{sh}}}{\tau_{\text{ac}}^{\text{SA}}} = \frac{3}{4\zeta\zeta'\beta_{\text{sh}}^2} \left(\frac{\tau_{\text{sc}}}{\tau_{\text{ac}}} \right) \sim 58 \times E_{50}^{0.1} \quad (21)$$

where we have used a relatively high Alfvén velocity of 1000 km/s, and set $\zeta = 10$ and $\zeta' = 1$. In spite of the relatively high Alfvén velocity *it appears that the conditions in the CME environment of delayed events favor re-acceleration of semi-relativistic electrons directly by turbulence rather than by the CME shock*. It should be noted that the above calculations are based on acceleration and scattering by parallel propagating waves. However, as mentioned above we expect similar results for obliquely propagating waves.

4. ACCELERATION OF He IONS

We now briefly address similar dichotomy that is observed in the characteristics of SEP ions. We will focus on relative spectra and abundances of ^3He and ^4He . Accelerated ions directed to the foot points of flaring loops produce γ -ray lines (and pions that decay into > 70 MeV gamma-rays). However, these are dominated by protons and in most flares cannot be used to determine the contributions of other ions. Thus, in the absence of detectable radiative signature for these ions we have only SEP spectral and temporal characteristics at our disposal. As mentioned in §1 there are differences similar to those found for electrons in the characteristics of ions; with shorter, weaker events (called “impulsive”) having softer spectra and higher enhancements of ^3He and heavy ions compared to, stronger, long duration (called “gradual”) events which are associated with fast CMEs (see e.g. Reames et al. 2014).¹¹

Here we explore the possibility of similar explanation with coronal acceleration of the impulsive SEPs and re-acceleration in the CME environment in stronger longer lasting events. Stochastic acceleration by turbulence has been the working hypothesis for gamma-ray producing ions (see, e.g. Ramaty & Murphy 1987) as well as some SEPs (see e.g. Mason et al. 1986; Mazur et al. 1992; Miller 2003; Ng & Reames 1994), but CMEs and the resultant shocks are believed to play important roles for gradual SEPs (Zank 2012).

One of the most vexing problems of SEPs has been the extreme enhancement of ^3He (e.g. Nitta et al. 2008). It was recognized early that the plasma wave-particle interactions and the unusual charge to mass ratio of ^3He could be the cause of such enhancements (see e.g. Fisk 1978 and other early works referred to in Petrosian et al. 2009). More recently, and with a more detailed treatment of the plasma wave interactions with ^3He and ^4He ions, Liu et al. (2004 and 2006) demonstrated that stochastic acceleration by turbulence can quantitatively explain both the extreme ^3He enhancement and the unusual shapes of ^3He spectra. Moreover, as shown in Petrosian et al. 2009, such a model can reproduce the large range of the observed ^3He to ^4He

¹¹It should be emphasized that there is no evidence for a impulsive-gradual or high-low enhancement bi-modality. As shown by Ho et al. (2005) (see also Petrosian et al. 2009) there is a broad continuum of ^3He to ^4He fluence ratio that decreases with increasing ^4He fluence.

fluence ratio. However, the pure stochastic acceleration model cannot explain the harder (characteristically broken power-law) spectra observed in the gradual events where there is little or no ^3He enrichments. Here we explore the possibility that these harder spectra arise because of re-acceleration in the CME environment.

Liu et al. (2004) showed that the spectra of He nuclei escaping the coronal acceleration site consist of a low energy quasi-thermal component (which is below the observable energy range of ~ 0.1 to 10 MeV/nucleon) and a higher energy nonthermal component with high ^3He enrichment. Liu et al. (2006) showed that the relative strength of the two components depends on many parameters but is most sensitive to the level of turbulence or $\tau_p^{-1} \propto f_{\text{turb}}$; at low levels of turbulence a small fraction of ^4He but most of ^3He is accelerated into a nonthermal tail. This explains the weak impulsive events with high enrichments. For higher levels of turbulence, expected to be the case for larger (and possibly more gradual) events, more of the quasi-thermal component of ^4He is moved to higher energies so that the ratio of ^3He to ^4He fluences (in the ~ 0.1 to 10 MeV/nucleon range) decreases eventually reaching normal coronal values. However, in higher fluence events *the model spectra* of ^4He , and to some extent that of ^3He , do not agree with the observed spectra of gradual events (As an example see the dashed model spectra and observed points in Fig. 7 below). Thus, the spectra coming out of the coronal acceleration site must be modified by a secondary process. Since high fluence events are more likely to be associated with fast CMEs, and hence strong shocks, then this modification can be due to re-acceleration in the CME environment. The most attractive feature of this scenario is that even though the nonthermal tails may be highly enriched, the total number of particles (quasi-thermal plus nonthermal) injected into this re-acceleration site can have essentially normal abundances. It should also be noted that, the shape of these seeds ions are qualitatively similar to the two (a steep low energy and flatter high energy) component model used by Tylka & Lee (2006) in their phenomenological description of the diffusive shock acceleration of SEPs. However, as mentioned above the origins of these seeds in our scenario is quite different than theirs, which assumes previously accelerated particle in the upstream of the shock. In our scenario the seed particles are the flare accelerated ions trapped behind the CME shock.

The equations describing the re-acceleration here is similar to those used above (Eqs. 16 and 17) for electrons. Again the losses can be ignored and we must be dealing with a strong diffusion case, but now the injected spectrum \dot{Q}' is not a simple power law but consists of a quasi-thermal plus a nonthermal component. Figure 7 (left) shows examples of re-accelerated spectra (red and blue points) from a simple shock (and/or stochastic acceleration) model with an injected thermal-plus-power-law spectrum (blue-dashed and solid-red curves) similar to those expected to emerge from the coronal acceleration site (see Liu et al. 2006). As evident, for reasonable values of the temperature of the quasi-thermal component and power-law indexes simple broken power laws emerge from the re-acceleration site. This demonstrates that a generic re-acceleration model can produce spectra similar to those observed in gradual events. However, a more accurate calculation using realistic parameters based on the conditions in the environment of the CME is required. Unfortunately these condition are poorly known. Nevertheless, as a more specific example in Figure 7 (right) we show a comparison between observation of a gradual SEP event and result from numerical solution of the full kinetic Equation (1) of re-accelerated ^4He and ^3He spectra using an examples of flare site accelerated spectra (from Liu et al. 2006) for the source term $\dot{Q}'(E)$. Here in addition to the diffusion term due to interaction with turbulence we have added a simple direct acceleration term, presumably by a shock that dominates at energies > 0.5 MeV /nucleon. As evident we get reasonable agreement. These are promising result but clearly more detail analysis is required to support this scenario.

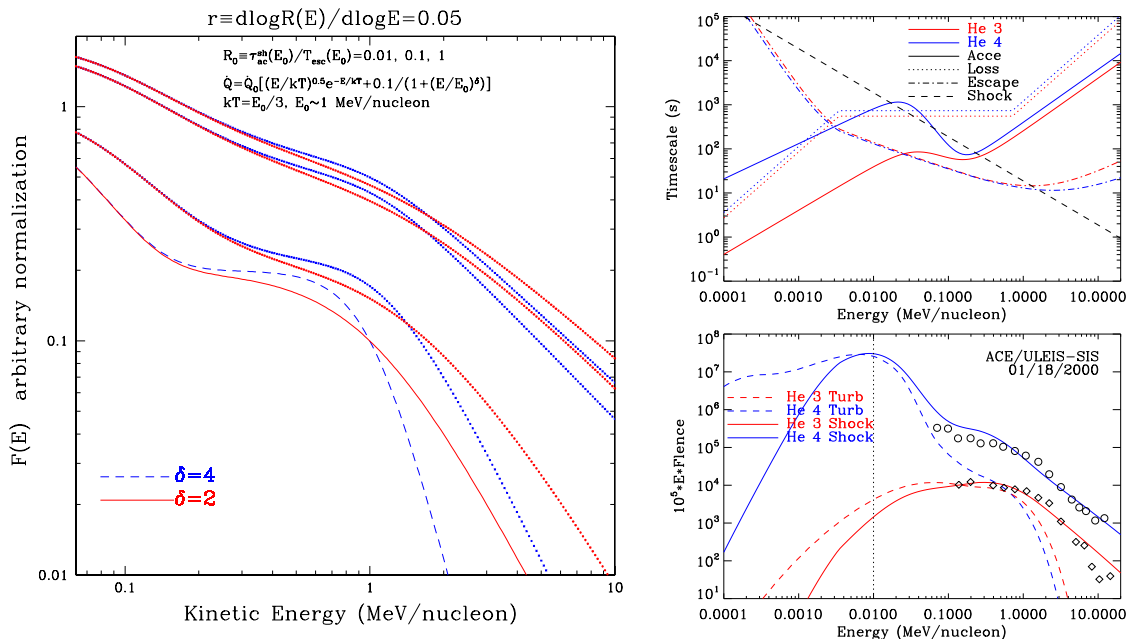


Fig. 7.— **Left:** Spectra of re-accelerated ions based on Equation (16) with a source term \dot{Q}' consisting of a thermal and a power-law component with the specified parameters with two spectral indexes $\delta = 2$ (red-solid and dots) and $\delta = 4$ (blue-dashed and crosses), and for three values of the ratio \mathcal{R}_0 from top to bottom. Note that for smaller values of \mathcal{R}_0 the spectra are modified into a broken power law form observed for ${}^4\text{He}$ and many other ions. **Right:** Fluence of ${}^4\text{He}$ (blue) and ${}^3\text{He}$ (red). The injected spectra from the flare acceleration site (from Liu et al. 2006) are shown by the dashed curves and the spectra of the re-accelerated ions are shown by the solid curves. The model timescales of the the stochastic plus shock acceleration in the CME environment are shown on the top panel. Stochastic acceleration timescales are from Liu et al. (2006) to which we have added an ad-hoc acceleration rate that dominates at energies > 0.5 MeV /nucleon, presumably due to a shock.

5. SUMMARY AND DISCUSSION

Several observations comparing the temporal and spectral characteristics of electrons responsible for the generation of solar flare nonthermal radiations (type III radio and HXR) with those of electrons seen as SEPs near the Earth indicate that the population can be roughly divided into two groups. In one group, referred to as “prompt” events, the SEPs appear to originate almost simultaneously with the radiations from the flare site located in low corona near the tops of reconnecting magnetic loops. HXR and SEP observations of a sample of flares analyzed by K07 shows that the HXR photon spectral index γ_{HXR} and the SEP spectral index δ_{SEP} are strongly correlated with the average relation $\delta_{\text{SEP}} \sim \gamma_{\text{HXR}}$. This relation does agree with either a thin or thick target model of the bremsstrahlung emission. Similarly, the total (time integrated) number of electrons required for production of HXR (based on the thick target model) N_{HXR} appears to also correlate (though somewhat more weakly) with the total number of observed SEP electrons N_{SEP} but the former is larger than the latter by 100 to 3000 times while the simplest model of common origin would imply comparable numbers. The second group referred to as “delayed” events show a complex temporal relation, often with the deduced time of emission of SEPs at the Sun coming after that of HXR or type III

radio. K07 data on 15 such events shows no or very weak correlation between the two indexes with the SEP index being smaller for all except one of the events. There is no information given on the relative number of electrons in the delayed events

A similar dichotomy seems to be present in the observations of SEP ions. Shorter, weaker events, often referred to as “impulsive” appear to have higher enrichment of ^3He and heavier than CNO ions and softer spectra with an unusual convex spectral shape for enriched ions. While longer duration and stronger events show near normal abundances and a harder broken power law spectra. Both the delayed electron and gradual-normal abundance ion events are more likely to be associated with a fast CME.

In this paper we address these dichotomies using the scenario that in the prompt and impulsive events particle acceleration takes predominately at the reconnecting coronal sites. But in the delayed-gradual events not only there is acceleration in the flare site but that these accelerated particles are re-accelerated in the CME-shock environment. This is different than the assumption made in most models of acceleration by a CME shock, where the seed particles are some yet unobserved nonthermal component of the upstream plasma. We quantify this model and show how such observations can be used to set constraints on the physical characteristics of the acceleration mechanism(s).

Our results can be summarized as follows:

- We first emphasize that the relation between radiation producing and SEP electrons is not simple so that the fluxes, numbers and spectra can not be assumed to be the same. In particular high resolution spectral and spatial HXR observation indicate that flare site acceleration is most likely located in the reconnection region just above the newly reconnected closed flare loops and the spectra and the rate of the escape of these particle to lower atmosphere where they produce the HXR could be different than that of the electrons escaping along open field lines to the Earth. Thus, a more careful analysis taking such differences into account is needed.
- We show that we can quantitatively account for the above mentioned observations using the simple leaky box model of acceleration, treating acceleration by plasma turbulence and shock at coronal reconnection and CME sites. The transport coefficients of this equation are related to two of the most basic characteristics common in all acceleration model, namely the momentum (or energy) and pitch angle diffusion coefficients and the background plasma characteristics (density, temperature, magnetic field strength and geometry). We convert the transport coefficients to their characteristics timescales; energy loss, energy gain or acceleration, energy diffusion times, and an escape time which depends on the scattering time, crossing time (across the acceleration site) and the magnetic field geometry. We describe an approximate but reliable method of quantifying these relations (Fig. 2). For the narrow range of electron energies of interest here (dictated by the limitations of the observations) we approximate the energy dependences of these time scales by power laws.
- Using the K07 data we show that the difference between delayed and prompt event spectral relations arises primarily because the differences in the SEP spectra and not the HXR spectra (Fig. 3); SEP spectra of delayed events are harder.
- Using the power law approximation we derive a simple relation between HXR and SEP indexes (Eq. 11) from which we derive the expected distribution of the index α_d of downward escaping time (Fig. 4) and show that the two flares for which CP13 obtained this index directly and non-parametrically from inversion of *RHESSI* data agree very well with this distribution. This strengthens the conjecture

of CP13 that in the flare acceleration site we are dealing with a weak spatial diffusion and a relatively strong field convergence in the downward direction.

- We also show that in this scenario the number of electrons required for production of HXR is larger than those observed near the Earth (mainly) by the ratio of energy loss time to downward escape time in the acceleration site. As shown in CP13 this ratio is much larger than one and depends on the one unknown parameter which is the density of electrons in the acceleration site. The observed ratio of 100 – 3000 indicates a density of about $\sim 10^9 \text{ cm}^{-3}$ which is about 10 times smaller than one gets from the plasma emission measure obtained from fitting to low energy thermal HXR.
- We then consider the re-acceleration in the CME-shock region (due to both stochastic and shock accelerations) and using analytic and numerical solutions of the kinetic equation to show that the harder SEP indexes of delayed events is consistent with this scenario and point how such observations (of individual and a population of events) can be used to constrain the re-acceleration rate and the escape time of SEPs from the CME-shock region. Using calculations based on interaction of electrons with waves of all modes propagating along the magnetic field lines we show that for the semi-relativistic electrons of interest here, stochastic acceleration by turbulence is more efficient than the expected low Alfvén Mach number shocks.
- Finally, we briefly consider a similar scenario to account for the differences between spectra and abundances of SEP ^3He and ^4He ions. Based on spectra obtained in the stochastic acceleration model of Liu et al. (2004 and 2006) we show that in general re-acceleration of such spectra can produce the characteristics harder broken power-law spectra seen in gradual events. Also using detailed numerical solution we fit the results from such a model to the observed spectra in one gradual event. This fit requires both diffusion and acceleration by turbulence and acceleration by a shock which becomes dominant at higher energies (Fig. 7).

In conclusion then we have demonstrated that with the scenario involving combined acceleration at the flare site and the CME environment we can explain some of the puzzling variations seen in spectra of SEP electrons and He ions and radiating electrons quantitatively. These results indicate that with more data and further more rigorous theoretical treatment we can begin to constrain some of the most important characteristics of the acceleration mechanism(s) in solar flares and answer many other questions that these results raise. For example, this scenario requires near simultaneous launch of a CME and acceleration at the reconnection site, and/or the trapping of the accelerated particles so that they interact with the CME. However, since number of SEP electrons are smaller than the radiating ones we require the trapping behind the CME shock of only a small fraction of flare accelerated electrons. Clearly the geometry of the magnetic fields extending from the reconnection site to the CME and characteristics of the turbulence generated behind the CME shock play important roles in this process. In general, all shock acceleration models require presence of turbulence both upstream and downstream of the shocks and some numerical simulations (see e.g. Giacalone & Jokipii 2007) show some indication of the presence of turbulence in the downstream region. These are important aspects that require extensive numerical simulations which are beyond the scope of this paper.

Acknowledgements: I would like to thank former graduate students, John Leach, James McTiernan and Qingrong Chen and Post doctoral fellow Siming Liu whose work contributed to the foundation of the results presented here. This work is supported by NASA LWS grant NNX13AF79G, H-SR grant NNX14AG03G and Fermi-GI grant NNX12AO78G. I would also like to thank an anonymous referee for some insightful

suggestions, G. Zank for pointing out the earlier work by Forman et al., and F. Effenberger for valuable comments.

A. ACCELERATED ELECTRON SPECTRA FROM TOTAL HXR SPECTRA

For spatially unresolved flares we have only the total HXR spectrum $J_{\text{tot}}(\epsilon)$ from which we can obtain the total spectrum of radiating electrons $N_{\text{tot}}(E)$ either by a forward fitting or by an inversion method (see Kontar et al. 2005) of an equation similar to Equation (7). As described in §3.1 the relation between this spectrum and that of the accelerated electrons $N(E)$ is not straightforward, especially at lower energies when there could be a significant emission from both loop top and footpoint sources. Here we demonstrate that, in principal, we can obtain the accelerated spectrum from $N_{\text{tot}}(E)$ if we have a knowledge of the energy dependence of the escape and energy loss times.

Normally $J(\epsilon)$ is considered to be a thick target spectrum from a single source. However, a more accurate description is that $J_{\text{tot}}(\epsilon) = J_{LT}(\epsilon) + J_{FPS}(\epsilon)$ is the sum of the *thin target* LT and the *thick target* emission from the loop outside the LT region, mainly from the FPs, with (volume integrated) electron spectra $N(E)$ and $N_{\text{eff}}(E)$ (Eq. 8), respectively. In other words the deduced total electron spectrum

$$N_{\text{tot}}(E) = N(E) + \frac{1}{\dot{E}_L} \int_E^\infty \frac{N(E')}{T_{\text{esc}}(E')} dE'. \quad (\text{A1})$$

The fact that $v\dot{E}_L$ is constant the differentiation of the above integral equation yields the differential equation

$$\frac{d(N/v)}{dE} - \frac{1}{\dot{E}_L T_{\text{esc}}} \frac{N}{v} = \frac{d(N_{\text{tot}}/v)}{dE}, \quad (\text{A2})$$

the solution of which gives the accelerated spectrum¹²

$$N(E) = N_{\text{tot}}(E) - v \int_{\eta(E)}^\infty \frac{N_{\text{tot}}}{v'} e^{\eta-\eta'} d\eta', \quad \text{with} \quad d\eta = \frac{dE}{\dot{E}_L T_{\text{esc}}} = \frac{\tau_L}{T_{\text{esc}}} \frac{dE}{E}, \quad (\text{A3})$$

with the second term giving the effective spectrum of Equation (9). Clearly the primary characteristics affecting this difference is the relation between η and E or the ratio $\mathcal{R}' = \tau_L(E)/T_{\text{esc}}(E)$, which is proportional to vE/τ_{sc} or $v^3 E \tau_{\text{sc}}$ in the weak and strong diffusion limits, respectively.

There are, however, some caveats. The simplicity of the above equations is somewhat deceiving. In equation (A2) we are required to take a derivative of the spectrum obtained from inversion of noisy data, which can limit the accuracy of the results.¹³ Note that even though Equation (A3) does not involve differentiation but integration (that tends to smooth out noise), it involves the subtraction of two nearly equal (noisy) terms which can amplify the noise. Nevertheless, this method is promising and with some judicious smoothing reasonable results can be obtained. Figure 8 shows an example where we obtain the accelerated spectrum $N(E)$ from the total spectrum obtained by Kontar et al. (2005) using regularized inversion of a *RHESSI* HXR spectrum, using the above equations and several energy (or velocity) dependence of T_{esc} . The difference $N_{\text{tot}} - N(E)$ gives the effective spectrum $N_{\text{eff}}(E)$. These then can be used to determine the other transport coefficients such as D_{EE} etc using the formalism described in CP13 (e.g. their Eq. (18)).

¹²Just a reminder that because the thick target footpoint emission is independent of density the energy loss time is calculated here using the density n_{LT} of the loop top acceleration site.

¹³Results obtained by inversion methods show that the errors in N_{tot} increase near sharp features (see Brown et al. 2006).

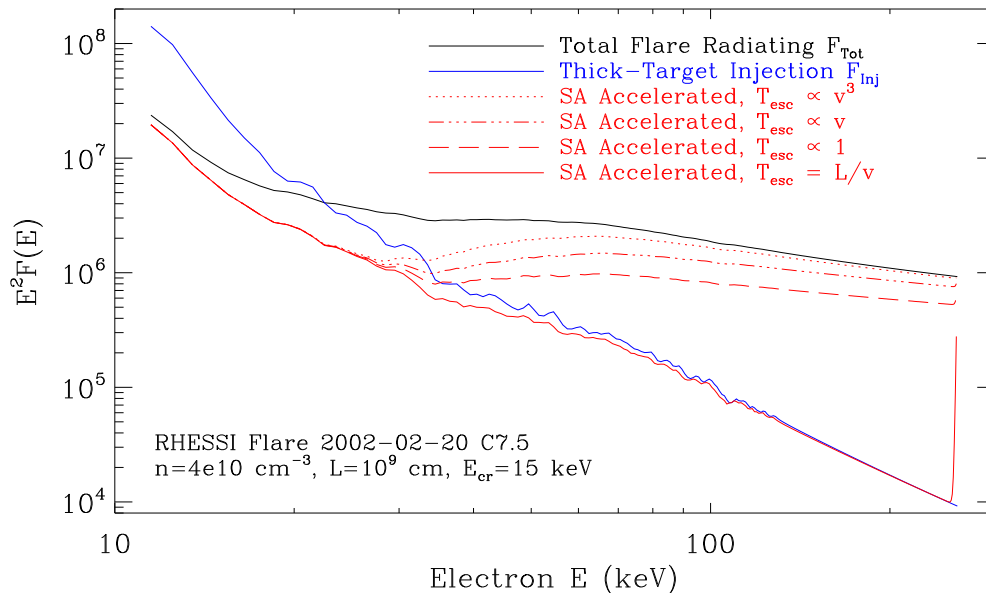


Fig. 8.— Demonstration of converting the total spectrum of the radiating $\bar{N}(E) = N_{\text{tot}}(E)$ (solid black curve, from Kontar et al. (2005)) to the accelerated spectrum $N(E)$ (shown by red solid, dotted and dashed curves) using Equation (A3) and various forms for the escape time. For comparison we also show the form of the injected spectrum assuming a simple thick-target model (steep blue solid curve). The curves for $N(E)$ can be used to obtain the energy dependences of the other transport coefficients such as D_{EE} and $A(E)$ as demonstrated in CP13 (see also Chen 2013 PhD Thesis Stanford University).

B. STOCHASTIC RE-ACCELERATION BY TURBULENCE

For stochastic acceleration by turbulence the diffusion and direct acceleration rates are comparable. Then ignoring the loss term the kinetic Equation 1 can be written as

$$\frac{d}{dE} \left[D_{EE} \left(\frac{dN}{dE} - \frac{N}{E} \xi \right) \right] - \frac{N}{T_{\text{esc}}} = \dot{Q}. \quad (\text{B1})$$

If we define an effective acceleration rate

$$A_{\text{eff}} = (\xi - d \log N / d \log E) D_{EE} / E \quad (\text{B2})$$

and assume that the slowly varying logarithmic derivative is constant then we get similar re-acceleration equation as for shock acceleration with this effective SA rate replacing A' in Equation (16) and same solutions as those presented in Figure 6 with the acceleration time

$$\tau_{\text{ac}}^{\text{SA}} = E / A_{\text{eff}} = \zeta' \tau_{\text{ac}} \quad \text{where} \quad \zeta' = \xi' / (\xi - d \log N / d \log E), \quad (\text{B3})$$

and $\tau_{\text{ac}} = p^2 / D_{pp}$ is the acceleration times calculated in PP97 and used in the text. As shown in Petrosian & Chen (2014) $\xi' = (\gamma + 1)(2\gamma^2 - 1) / \gamma^3 \sim 2$ for all energies. For sub-relativistic regime under consideration here $\xi \sim 0.5$ and from observations we estimate $d \log N / d \log E \sim -1$ to -3 so that the correction coefficient ζ' varies between 1.33 to 0.8.

C. RE-ACCELERATED SPECTRA FOR $r = 0$

Many treatment of the acceleration use the simplifying assumption of energy independent escape and acceleration times or rate) which is an special case of when the acceleration and escape time have similar energy dependence and the ratio \mathcal{R}_0 is constant. This gives $\eta = \mathcal{R}_0 \ln(E/E_0)$ and $e^\eta = (E/E_0)_0^{\mathcal{R}_0}$. Substituting this in Equation (16) it is easy to show that for a power law injected spectrum $\dot{Q}(E) = \dot{Q}_0(e/E_0)^\delta$ we get

$$F(E) = \frac{\dot{Q}_0 \mathcal{R}_0}{\delta - \mathcal{R}_0 - 1} (x^{-\mathcal{R}_0 - 1} - x^{-\delta}) + F(E_0), \quad \text{where } x = E/E_0. \quad (\text{C1})$$

For $\mathcal{R}_0 > \delta - 1$, i.e. when the acceleration time is longer than the escape time the spectrum asymptotically approaches the injected spectrum $F \propto x^{-\delta}$, and in the opposite case of $\mathcal{R}_0 < \delta - 1$, i.e. shorter acceleration time, $F \propto x^{-\mathcal{R}_0 - 1}$ so that the re-accelerated spectrum becomes harder (index changing by $\delta - \mathcal{R}_0 - 1$). Thus, for typical index change of 1 we need $\mathcal{R}_0 = 1(2)$ for injected index $\delta = 3(4)$.

REFERENCES

- Ackermann Ajello, M., Allafort, A., et al. 2012, ApJ, 745, 144
 Ackermann, M., Ajello, M., Albert, A., et al. 2014 ApJ, 787, 15
 Ajello, M., Albert, A., Allafort, A. et al. 2014 ApJ, 789, 20
 Brown, J. C. 1972, Sol. Phys., 25, 118
 Brown, J. C. et al. 2006, ApJ, 643, 523
 Chen, Q. 2013, PhD Thesis, Stanford University <https://pur1.stanford.edu/mh246zj4146>
 Chen, Q., & Petrosian, V. 2013, ApJ, 777, 33; (CP13)
 Chupp, E. L., Forrest, D. J., Ryan, J. M. et al. 1982, ApJ, 263, L95
 Chupp, E. L., & Ryan, J. M. 2009, Res. in Ast & Astrophys. 9, 11
 Drake, J. F., Swisdak, M., Che, H., & Shay, M. A. 2006, Nature, 443, 553
 Drake, J. F., Swisdak, M., & Ferno, R. 2013, ApJ, 763, L5
 Fisk, L. A. 1978, ApJ, 224, 1048
 Forman, M. A., Webb, G. M., & Axford, W. I. 1981, ICRC, 9, 238
 Giacalone, J., & Jokipii, J. R. 2007, ApJ, 663, L41
 Gopalswamy, N., & Yashiro, S. 2011, ApJ, 736, L17
 Guo, F. & Giacalone, J., 2012, ApJ, 753, 28
 Haggerty, D. K., & Roelof, E. C. 2002, ApJ, 579, 841
 Ho, G. C., Roelof, E. C., & Mason G. M. 2005, ApJ, 621, L141
 Hurford, G. J., Schwartz, R. A., Krucker, S., Lin, R. P., Smith, D. M. & Vilmer, N. 2003, ApJ, 595, L77
 Jokipii, J. R., & Giacalone, J. 1996 Space Sci. Rev., 78, 137
 Klein, K.-L., Krucker, S., Trottet, G., & Hoang, S. 2005, A&A, 431, 10
 Koch, H. W. & Motz, J. W. 1959, Rev. Modern Phys., 31, 920
 Kontar, E. P., Emslie, A. G., Piana, M. et al. 2005, Sol. Phys., 226, 317 M.
 Krucker, S., Larson, D. E., Lin, R. P., & Thompson, B. J. 1999, ApJ, 519, 864

- Krucker, S., Kontar, E. P., Christe, S., & Lin, R. P. 2007, *ApJ*, 663, L109 (**K07**)
- Krucker, S., & Lin, R. P. 2008, *ApJ*, 673, 1181
- Le Roux, J. A., Zank, G. P., Webb, G. M., & Khabarova, 2015, *ApJ*, 801, 112
- Le, A., Karimabadi, H., Egedal, J., Roytershteyu, v., & Daughton, W. 2012, *Plasma Phys.*, 19, 072120
- Lee, M.A., *ApJS*, 158, 38, 2005
- Lin, R. P., Dennis, B. R., & Hurford, G. J. 2002, *Sol. Phys.*, 210, 3
- Lin, R. P., & Hudson, H. C. 1971, *Sol. Phys.*, 17, 412
- Liu, S., Petrosian, V., & Mason, G. M. 2004, *ApJ*, 613, L81
- Liu, S., Petrosian, V., & Mason, G. M. 2006, *ApJ*, 636, 462
- Liu, W., Petrosian, V., Dennis, B. R., & Jiang, Y. W. 2008, *ApJ*, 676, 704
- Liu, W., Chen, Q., & Petrosian, V. 2013, *ApJ*, 767, 168
- Maia, D. J. F., & Pick, M. 2004, *ApJ*, 609, 1082
- Mason, G. M., Reames, D. V., von Rosenvinge, T. T., Klecker, B., & Hovestadt, D. 1986, *ApJ*, 303, 849
- Malyshkin, L. & Kulsrud, R. 2001, *ApJ*, 549, 404
- Mason, G. M., Dwyer, J. R., & Mazur, J. E. 2000, *ApJ*545, 157L
- Mason, G. M. et al. 2002, *ApJ*574, 1039
- Masuda, S., Kosugi, T., Hara, H., Tsuneta, S., & Ogawara, Y. 1994, *Nature*, 371, 495
- Mazur, J. E. et al. 1992, *ApJ*401, 398
- Melissa Pesce-Rollins, Nicola Omodei, Vahé Petrosian, Wei Liu, Fatima Rubio da Costa, Alice Allafort, Qingrong Chen, 2015 *ApJ*, 805. 15
- Miller, J. A., LaRosa, T.N., & Moore, R.L. 1996, *ApJ*445, 464
- Miller, J. A. 2003, *COSPAR Colloquia Series* Vol. 13, 387
- Ng, C. K., & Reames, D. V. 1994, *ApJ*, 424, 1032
- Nitta, N. V., Freeland, S. L., & Liu, W. 2010, *ApJ*, 725, L28
- Oka, M., Phan, T.-D., Krucker, S., Fujimoto, M. & Shinokava, I. 2010, *ApJ*, 714, 915
- Parker, L. N., & Zank, G. P. 2012, *ApJ*, 757, 97
- Petrosian, V. 1973, *ApJ*, 186, 291
- Petrosian, V. 1982, *ApJ*, 255, L85
- Petrosian, V. 2012, *Space Sci Rev.*, 173, 535
- Petrosian, V., & Kang, B. 2015, *ApJ*, 813, 5
- Petrosian, V., & Donaghy, T. Q. 1999, *ApJ*, 527, 945
- Petrosian, V., Donaghy, T. Q., & McTiernan, J. M. 2002, *ApJ*, 569, 459
- Petrosian, V., & Liu, S. 2004, *ApJ*, 610, 550
- Petrosian, V., Jiang, Y. W., Liu, S., Ho, G. C., & Mason, G. M. 2009, *ApJ*, 701, 1
- Piana, M., Massone, A. M., Kontar, E. P., et al. 2003, *ApJ*, 595, L127
- Pryadko, J. M., & Petrosian, V. 1997, *ApJ*, 482, 774 (**PP97**)
- Pryadko, J. M., & Petrosian, V. 1998, *ApJ*, 495, 377

- Pryadko, J. M., & Petrosian, V. 1999, *ApJ*, 515, 873
- Ramaty, R., & Murphy, R. J. 1987, *Space Sci. Rev.*, 45, 213
- Reames, D. V., Meyer, J. P., & von Rosenvinge, T. T. 1994, *ApJS*, 90, 649
- Reames, D. V. 2013, *Sp. Sci. Review*, 175, 53refer Reames, D. V. et al. 1997, *ApJ*483, 515
- Reames, D. V., Cliver, E. W., & Kahler, S. W. 2014, *Sol. Phys.*, 289, 4675
- Russell, R. T., & Mulligan, T. 2002, *Planet. Space Sci.*, 50, 52
- Schlickeiser, R. 1989, *ApJ*, 336, 243
- Steinacker, J., Schlickeiser, R., & Droge, W. 1988, *Sol. Phys.*, 115, 313
- Tylka, A. J., & Lee, M. A. 2006, *ApJ*, 646, 1319
- Wang, L., Lin, R. P., Krucker, S., & Mason, G. 2012, *ApJ*, 759, 69
- Zank, G. P., Le Roux, J. A., Webb, G. M., Dosch, A., & Khoborova, d. 2014, *ApJ*, 797, 28
- Zank, G. P., Hunana, P., Mostafavi, P., Le Roux, J. A., Li, Gang, Webb, G. M., Khabarova, O., Cummings, A., Stone, E., & Decker, R, 2015 *ApJ*, 814, 28